COBEM 2023 27TH INTERNATIONAL CONGRESS OF MECHANICAL ENGENEERING

ABCM Brazilian Society of Mechanical Sciences and Engineering
27th ABCM International Congress of Mechanical Engineering
December 04-08, 2023, Florianópolis-SC, Brazil

COB-2023-0252
NUMERICAL ANALYSIS OF THE FLOW OVER AN E-VTOL CONCEPT VEHICLE

Gabriel Cicelini
Odenir de Almeida
Experimental Aerodynamics Research Center (CPAERO) - Federal University of Uberlandia (UFU), Rod 050 Km 78
gabrielcicelini@ufu.br
odenir.almeida@ufu.br

Abstract. *Aerial vehicles called e-VTOL's (electric vertical take-off and landing vehicles) promise to be the future of urban transport of people and products. Companies from different countries study and develop their own models, always prioritizing energy efficiency and aerodynamics. This work presents a CFD analysis of a conceptual e-VTOL based on existing models and/or prototypes. Simulations are implemented using Navier-Stokes equations (RANS) in the Ansys software with the two-equation realizable k-ε and k-ω turbulence models; the mesh was constructed of tri and tetrahedral elements passing through a refinement process. The computational solution was prepared for a scaled-model, at lower relative air speeds, around 20 meters per second, consistent with the flight of an e-VTOL. The similarity of the numerical results with some experimental data is discussed, obtaining a good level of coherence between the data. The investigation of the effects of changes in geometry, as well as the proposal of new designs and concepts, are suggested for future work.*

Keywords: *e-VTOL, CFD, turbulence models simulation, RANS*

1. INTRODUCTION

The concept of an aircraft that could take off and land without needing a relatively long runaway arouse the attention of those concerned about the urban mobility. The urban transport modal of great megalopolises around the world could take advantage of VTOL (Vertical Take-off and Landing) aircrafts. Since one of the main concerns of the humankind nowadays is the reduction in emissions of pollutants resulting from the burning of fossil fuels, the concept of Electric Vertical Take-Off and Landing aircrafts (e-VTOLs), took place as the main goal of several companies and joint ventures. The main idea behind many of these projects is to make air-taxi operations a reality, so they can work in conjunction with current urban transport systems, always prioritizing safety, sustainability, and efficiency.

The development of e-VTOL aircrafts is a completely new path to be trodden, and it will present new challenges in addition to those requirements already known by the big companies in the aviation branch. These challenges have been noted by those who search to develop new concept e-VTOL aircrafts, like the autonomy of the power supply (batteries), the possibility of autonomous piloting, acoustic footprint, safety issues and how to diminish them, and many others.

Among the designs currently presented by the leading companies in that segment, some are more attractive than others. Figure 1 describes some e-VTOL vehicles being pursued by different aircraft's manufactures around the world. Those who present low rotor configuration, for example, convey the feeling that accidents could occur when a passenger tries to get to the cabin. Also, the concepts endowed with conventional wings in addition to the rotors tend to transmit a feeling of trust for offering a glide ratio in case of engine failure, while the projects that present drone configuration do not provide this additional safety feature. According to Stoll et al. (2014), the Distributed Electric Propulsion (DEP) system is another feature that contributes to the overall efficiency of the vehicle, especially when dealing with small aircrafts, like the one proposed by this thesis.

The study of e-VTOL concepts and the flow-structure interactions had been mostly conducted in an industrial environment. Therefore, there is a relatively small number of articles regarding this topic. However, as the e-VTOL study advances towards a tangible reality, is expected that more analysis will be taking place among the academics and hopefully, it will lead to the emerging of new technologies. With all the variety of designs proposed for e-VTOL concepts, the question about which would be the best configuration appears. Bacchini and Cestino (2019) discussed the advantages and disadvantages of all different categories, from the first concepts developed in the fifties and sixties to the present e-VTOL configurations. In a more practical analysis, they selected three aircrafts (E-Hang 184, Wisk Cora and Lilium) and estimated several dimensions of each concept through pictures. The data was used to build up information like the total energy required for a considered mission and the drag polar of each aircraft. This study revealed that the best e-VTOL configuration depends on the mission, once short-ranged missions are best fitted by multirotor designs due to the better hover performance, while long range missions require more range capability.

The aerodynamic modeling of an e-VTOL concept is also a complex process. Simmons and Murphy (2021) recently conducted the implementation of a methodology to develop a high-fidelity aerodynamic model for the Langley

Aerodrome No. 8 (LA-8), a tandem tilt-wing, distributed electric propulsion e-VTOL concept. Two novel system identification-based approaches were used to develop an aerodynamic model for the LA-8 vehicle using wind tunnel data. The modeling strategies were compared by assessing their predictive performance for validation data acquired separately from the data used to identify the model, and a sufficient predictive capability was proven.

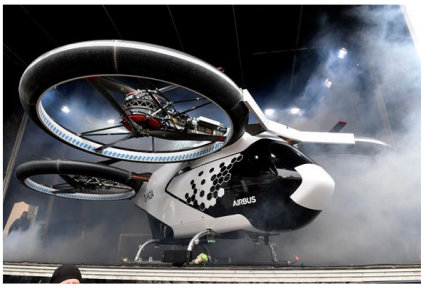

(a) CityAirbus
Fonte: https://evtol.news/airbus-helicopters/, 2023.

(b) Archer Midnight
Fonte: https://www.archer.com/midnight, 2023.

(c) Ehang-216
Fonte: https://www.helicopterspecs.com/2019/10/ehang-216.html, 2023.

(d) Ehang-vt30
Fonte: https://evtol.news/ehang-vt30, 2023.

(e) Eve Air Mobility
Fonte: https://evtol.news/embraer/, 2023.

(f) Cavorite
Fonte: https://evtol.news/horizon-aircraft-cavorite-x5, 2023.

(g) Joby-s4
Fonte: https://evtol.news/joby-s4, 2023.

(h) Lilium Jet
Fonte: https://evtol.news/lilium/, 2023.

(i) Terrafugia
Fonte: https://evtol.news/terrafugia-tf-2a/, 2023.

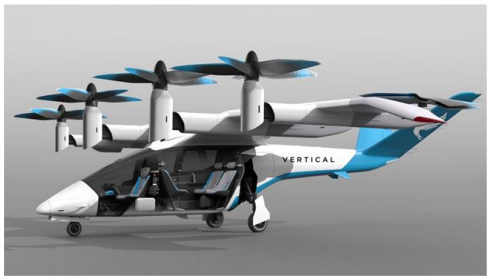

(j) Vertical Aerospace VA-1
Fonte: https://evtol.news/vertical-aerospace-VA-1X, 2023.

(l) Volocopter
Fonte: https://evtol.news/volocopter-volocity/, 2023.

(m) Wisk Cora
Fonte: https://wisk.aero/aircraft/, 2023.

Figure 1. E-VTOL concept vehicles around the world.

The motivation for this work is to analyze different kinds of e-VTOL designs presented by different companies nowadays, aiming to develop a new concept that brings around the best features observed in the most promising designs. Characteristics as the construction materials, dimensions, passenger capacity, range, cruise speed and many others, will guide the parsing. A numerical analysis will be conducted in a commercial CFD software, where the scaled model will be submitted to a flight condition and the results will be compared at the end. A new e-VTOL concept, as said, will be confronted with many challenges, and this work will focus on the aerodynamic analysis of a prototype. The interaction between wing and the propulsion system, the flow behavior over the vehicle's body as well as the basic aerodynamic parameters evaluation intend to make possible the development of a promising design capable of face the real-world requirements.

2. E-VTOL CONCEPT

Before the definition of which characteristics will be applied in the concept of this study, it is convenient to analyze the main technical features observable in all the e-VTOLs mentioned earlier. The following table diagrammatize the most important characteristics in each model.

Table 1. Main features of current e-VTOL's in market.

Vehicle	Layout Configuration	Wing Position	Propulsion System	Number of Occupants	Tilting Components	Landing Gear
Airbus CityAirbus	Drone	-	DEP	4	No	Fixed skid
Archer (Unnamed)	Wing	High	DEP	5	Yes	Fixed tricycle
EHang 216	Drone	-	DEP	2	No	Fixed skid
EHang VT-30	Wing	Low	DEP	2	No	Fixed tricycle
EmbraerX Eve	Wing (canard)	High	DEP	4	No	Fixed skid
Horizon Aircraft Cavourite X5	Wing (canard)	Low	Distributed (Hybrid)	5	No	Retractable tricycle
Joby S4	Wing	High	DEP	5	Yes	Retractable tricycle
Lillium Jet	Wing (canard)	Mid	DEP	5	Yes	Fixed tricycle
Terrafugia TF-2A	Wing	High	DEP	3	No	Fixed tricycle
Vertical Aerospace VA-X4	Wing	High	DEP	5	Yes	Retractable tricycle
Volocopter VoloCity	Drone	-	DEP	2	No	Fixed skid
Wisk Cora	Wing	Low	DEP	2	No	Fixed tricycle

Most of the concepts presented in the table have a wing configuration, combined with the DEP system. This layout delivers a more efficient horizontal flight since it takes advantage of the aerodynamic properties of the wing. It also eliminates the necessity of moving parts since the vehicle usually have rotors for the VTOL operation and an additional propeller for horizontal flight. All the different layouts show that those with high wing configuration, with the rotors out of range for the occupants, propose a safer design. Reducing the risk of accidents involving people hitting in-movement rotors is one of the objectives of the new concept to be presented. Regarding the landing gear system, there are advantages and disadvantages of each type. A retractable landing gear reduces drag while in flight but adds moving parts that can present malfunctioning and makes the maintenance more laborious. A fixed landing gear, although it provides more drag, makes up for being easier to maintain and operate, beyond reducing the project's financial cost.

With all those considerations, the baseline geometry chosen for this study was a mix of Wisk Cora and Terrafugia TF-2A designs. Both concepts gather most of the desirable characteristics in an e-VTOL project and the 3-view blueprint of the Wisk Cora was found in online database, making it easier to build a detailed printable model in the CAD environment.

2.1 3D sizing and design

Gathering all the defined features, dimensions and specifications stated until this point, a model was developed with the use of the CATIA v5. The 3-view projection of Wisk Cora was used to guide the lines of this concept, which presents all the modifications intended to improve the original design. The result is shown below in Figure 2. The detailed dimensions of the real scale model are available in sequence:

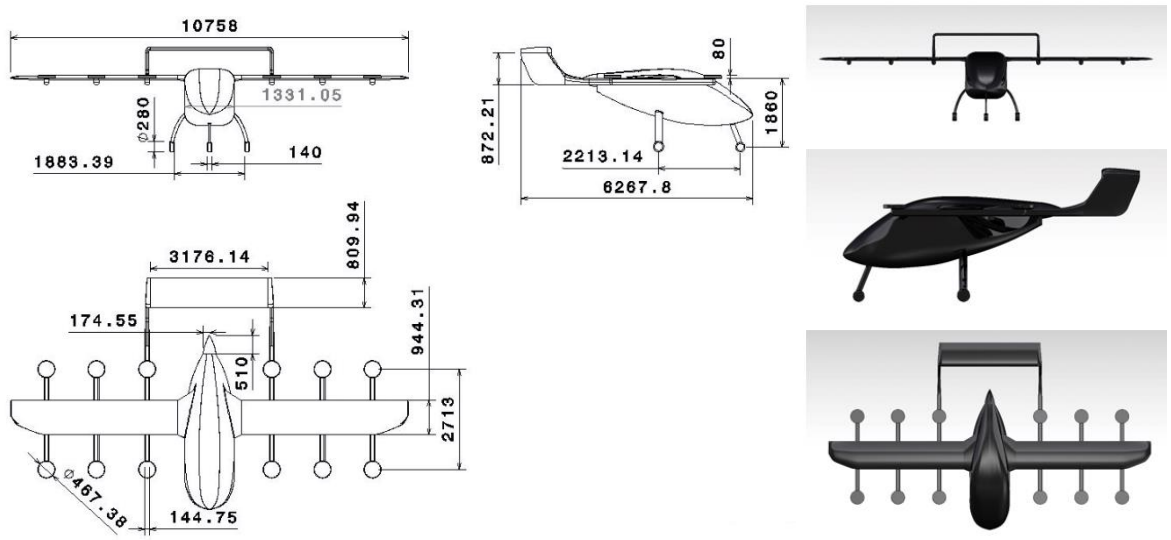

Figure 2. The e-VTOL concept elaborated in CAD environment.

As it is possible to verify by the pictures, the vertical flight rotors were simplified as discs and the rear propeller blades were not included in this construction, intending to eliminate undesirable variables in the experimental and numerical analysis. A comparison of sizes shows that, as intended, an average-sized person walking by or entering the aircraft will not have to worry about the rotors, for they will occupy a higher position when the e-VTOL is on the ground – Figure 3. However, this will bring another issue, which is the necessity of a retractable step to help passengers to get on board.

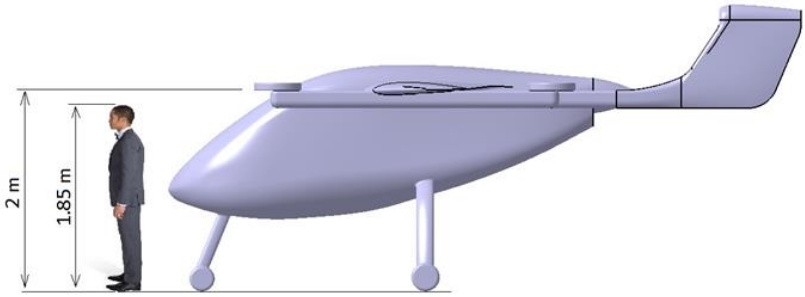

Figure 3. Size comparison between the e-VTOL and an average-sized human being.

3. NUMERICAL ANALYSIS

This section aims to present the settings of the numerical analysis implemented in this work. Here are explained the computational domain discretized for the process and other important information relative to the numerical simulation procedure.

3.1 CFD solver

In this computational analysis, the ANSYS FLUENT was employed. A pressure-based solver was chosen, operating with double precision. The Realizable k-epsilon model was utilized as the turbulence model for this analysis, which is a two-equation RANS model designed to predict flow separation on smooth surfaces. Incompressible air was specified as the working fluid for the fluid flow within the domain. The pressure-velocity coupling was handled using the SIMPLE algorithm.

3.2 Turbulence modeling and Reference Conditions

As mentioned, the implemented turbulence model was the RANS Two-Equation Realizable k-ε. It consists in a two-equation model that gives a general description of turbulence by means of partial differential equations:

$$\frac{\partial}{\partial t}(\rho k) + \frac{\partial}{\partial x_j}(\rho k u_j) = \frac{\partial}{\partial x_j}\left[\left(\mu + \frac{\mu_t}{\sigma_k}\right)\frac{\partial k}{\partial x_j}\right] + G_k + G_b - \rho\epsilon - Y_M + S_k \tag{1}$$

and

$$\frac{\partial}{\partial t}(\rho \epsilon) + \frac{\partial}{\partial x_j}(\rho \epsilon u_j) = \frac{\partial}{\partial x_j}\left[\left(\mu + \frac{\mu_t}{\sigma_\epsilon}\right)\frac{\partial \epsilon}{\partial x_j}\right] + \rho C_1 S_\epsilon - \rho C_2 \frac{\epsilon^2}{k+\sqrt{\nu\epsilon}} + C_{1\epsilon}\frac{\epsilon}{k}C_{3\epsilon}G_b + S_\epsilon \tag{2}$$

where

$$C_1 = max\left[0.43, \frac{\eta}{\eta+5}\right], \quad \eta = S\frac{k}{\epsilon}, \quad S = \sqrt{2S_{ij}S_{ij}} \tag{3}$$

As described by Ansys Fluent User's Guide (2016), G_k represents the generation of turbulence kinetic energy due to the mean velocity gradients. G_b is the generation of turbulence kinetic energy due to buoyancy. Y_M represents the contribution of the fluctuating dilatation in compressible turbulence to the overall dissipation rate. C_2 and $C_{1\epsilon}$ are constants. σ_k and σ_ϵ are the turbulent Prandtl numbers for k and ε, respectively. S_k and S_ϵ are user-defined source terms. Additional details can be seen in Ansys Fluent User's Guide (2016).

It is known that the Realizable k-ε is the default recommendation in mainstream commercial packages, therefore represents the most proven, well-quantified and widely documented of all closures. The model has improved performance for planar surfaces, round jets, rotation, recirculation and streamline curvature.

Table 2 summarizes the reference conditions used in the simulations.

Table 2. Reference conditions for simulations.

Property	Representation	Value
Geometry	S/2	0.003 m^2
	L	0.232 m
Fluid	ρ_∞	1.154 kg/m^3
	μ_∞	1.899×10^{-5} kg/m.s
Flow	α (AOA)	0°
	U_∞	20.0 m/s
	Re	2.820×10^5

3.3 Computational Domain and Boundary Conditions

The computational domain was defined for half-model, saving computational effort. The domain frontiers were defined in a distance such that the flow field around the body would suffer no influence of the borders. All the distances used to define the dimensions of the domain were based on the actual length of the scale model, which is L = 231.91 mm. Basically, the domain consists of a quarter sphere ahead of the model, with a half cylinder developed backwards, starting from the semicircle face of the quarter sphere. It all becomes clearer in Figure 4. The sizing of the computational domain was based on previous work of Almeida and Souza (2017) which presented no influence of the boundary conditions on the results.

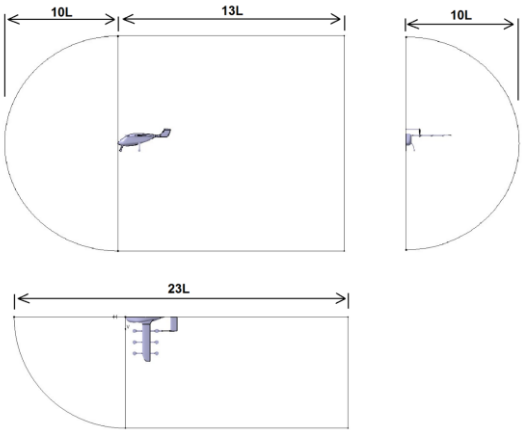

Figure 4. Three views with dimensions of the computational domain. This representation is out of scale for better visualization.

The appropriate boundary conditions were applied to this computational model as described: the whole surface of the aircraft is a non-slip wall; the entry of the domain and the lateral boundaries in the cylindrical part was set as a farfield condition where the flight speed and ambient values were set; the boundary that splits the domain as a half was set to symmetry and at the rear of the domain an outflow condition was adjusted.

3.4 Mesh

The proposed architecture to build a good mesh was based in some main regions, to have specific refinement, separated in the computational domain, which are: 1) The far field; 2) The near field; 3) The inflation; 4) The surface of the aircraft; and 5) Refinement spheres.

The near field domain consists of a geometric boundary (virtual density box) involving the aircraft, aiming to provide a smooth transition of the mesh size, from the far field to the surface of the model. The inflation is made of layers immediately above the surface of the model. The wall spacing between the elements of the inflation was computed through the following parameters – Table 3:

Table 3. Reference parameters for inflation wall spacing calculation.

Freestream Velocity (U_∞) [m/s]	**Freestream Density (ρ) [kg/m^3]**	**Dynamic Viscosity (μ) [kg/m.s]**	**Reference Length (L) [m]**	**Y^+**
20.0	1.1542	1.899×10^{-5}	0.2319	30.0

These numbers resulted in a wall spacing $\Delta S = 0.5305$ mm through the Y+ calculation procedure. Due to the characteristics of the CAD model, which includes small ratio curvatures and other features difficult to mesh, the number of piled layers composing the inflation was maintained in a total of six. The surface of the aircraft was always slightly more refined than the near field, so it is intended to reproduce the effects of the pressure gradient and wall shear observed experimentally – Cicelini (2022).

To maintain the orthogonal quality and the skewness of the mesh elements within an acceptable margin (above 0.1 and below 0.95, respectively), some regions of the model needed extra-refining. This way, refinement spheres were strategically positioned to contain those problematic spots and hold those parameters in acceptable values.

A coherent analysis of the flow behavior related to the aircraft model requires a mesh that is properly refined. Ideally, a more refined mesh will undoubtedly provide better results, but for that there is a high price in terms of computational cost. This way, it is necessary to achieve a mesh considered both sufficient to provide a coherent result and viable regarding the computational effort.

With that in mind, three meshes were developed starting from an original 6.4 million elements mesh. The characteristics of each one is related in Table 4. By following it, a sequence of three images shows how Mesh 2 looks like – Figure 5. The CFD calculations were performed in a workstation with an Intel Core i7-3930K (3.20 GHz) processor with twelve cores (six physical) and 48.0 GB RAM memory.

Table 4. Mesh configurations.

Mesh	Refining Factor	Number of Elements	Elapsed Time [min]
Mesh 1	1.183216	2,698,745	161
Mesh 2	1	6,422,799	406
Mesh 3	0.707107	10,100,767	989

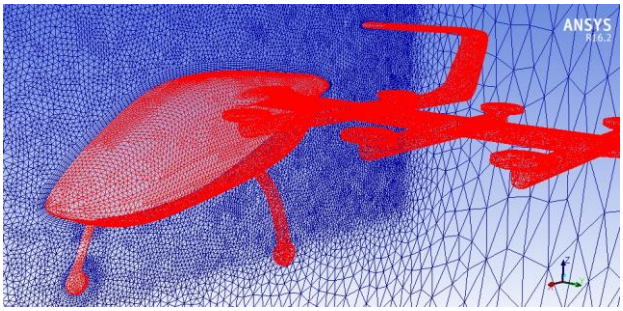

(a) A general overview

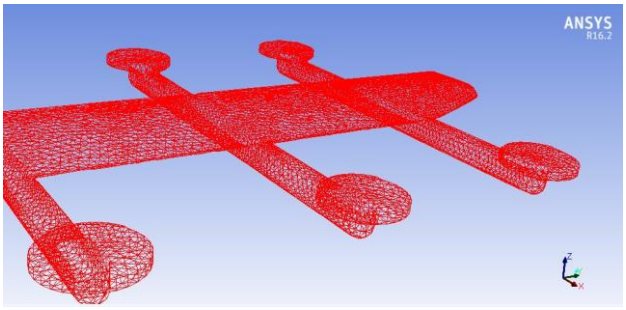

(b) A close view of the mesh around engine supports.

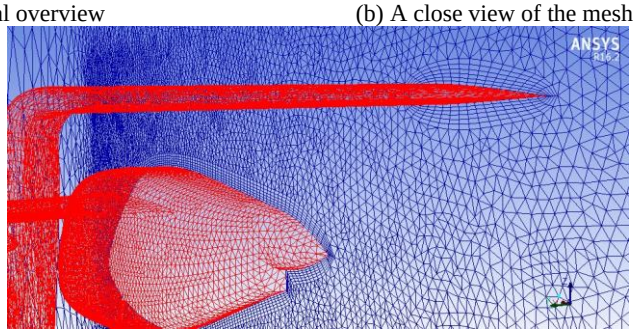

(c) A close view of the inflation layer intersected with the symmetry plane.

Figure 5. Details of the mesh refinement procedure.

4. RESULTS AND DISCUSSION

This section presents the numerical results from CFD simulations. The results are intentionally disposed in an order where it is possible to use some experimental data from Cicelini (2022) for comparison reasons. First, the mesh convergence criteria are verified, aerodynamic parameters such as pressure distribution, velocity profiles are checked, and a characterization of the flow field is achieved by means of contours plots.

4.1 Mesh Convergence

The first simulations aimed to define which one of the three developed meshes was more adequate to this study. The main factors, as it was stated, were computational cost and reliability. The computed results used to this comparison were the drag and lift coefficients calculation, after 2000 iterations. As seen in Table 4, the elapsed time for the three meshes were very distinct. The converged values from each simulation were obtained and compared to verify mesh convergence to a stable and repeatable single value with a reasonable computational time, which is shown in Table 5.

The results show a small deviation from Mesh 2 to Mesh 3 in terms of C_D and C_L values while the computational time is more than twice. From this, it is possible to conclude that Mesh 2 fulfill the reliability criteria, in addition to be more viable from the point of view of computational effort, as observed in Table 4. The subsequent analysis will be based on results obtained from simulations using Mesh 2.

Table 5. Mesh convergence data.

Property	Mesh 1	Mesh 2	Mesh 3	Relative deviation Mesh 1 to 2	Relative deviation Mesh 2 to 3
C_D	0.264	0.247	0.243	6.8%	1.4%
C_L	0.081	0.089	0.089	10.1%	0.4%

4.2 Aerodynamic parameters

The following graphic – Figure 6 shows the data acquired by post-processing the CFD results, referring to the pressure profile on the fuselage centerline in terms of pressure coefficient (Cp). The reference line matches the symmetry line of the model, going from the fuselage apex, which is the origin, in direction to the spinner in the rear part of the model.

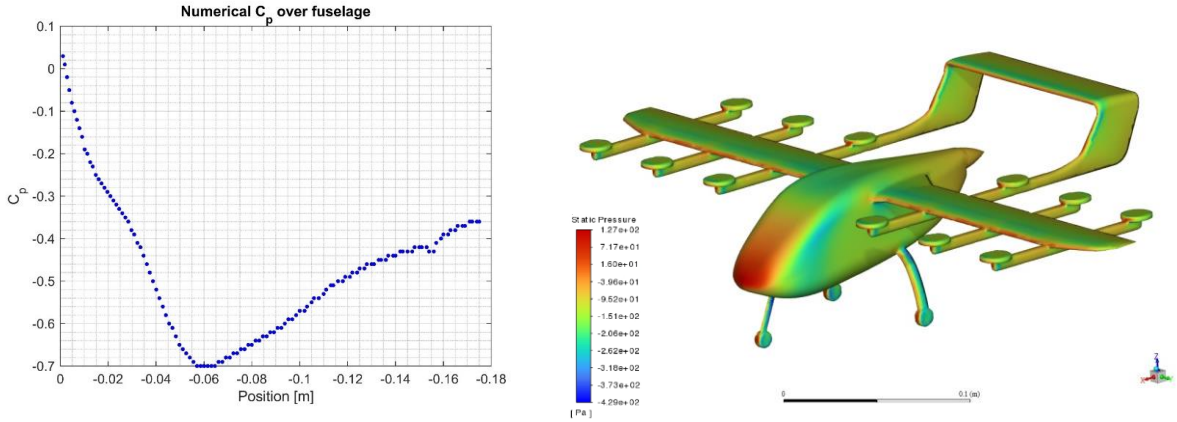

(a) (b)

Figure 6. Pressure distribution over the fuselage: (a) Cp distribution; (b) Static Pressure.

The behavior of the pressure coefficient curve above can be explained by the smooth decay of pressure and the subsequent recovery (also smooth) over the fuselage. That is, it is very similar to the Cp values over an airfoil at moderate angle of attack (AOA). It is important to mention that the AOA was kept 0º degrees, as registered in Table 2 and in this operational condition the flow is completely attached over the fuselage (Fig.6(b)).

A subsequent analysis was to obtain the velocity profiles taken behind the propulsion system, including the pods and main engine mounted on the rear of fuselage. A rake of 13 points vertically and equally spaced was repeated at three different locations, as seen on Fig. 7. The horizontal distance was set to be 116 mm between the trailing edge of the horizontal stabilizer and the probes. That is the length of the model divided by 2. The vertical position was also fixed, in a way that the 7th and central probe was aligned to the trailing edge of the horizontal stabilizer.

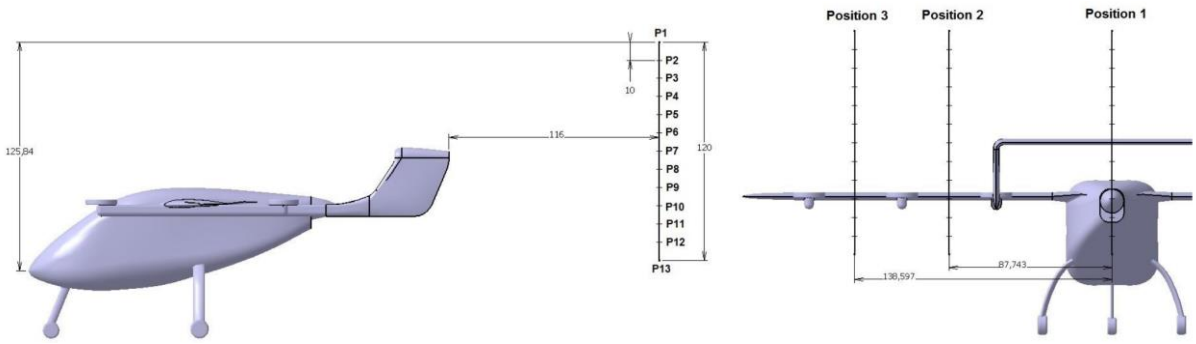

Figure 7. Rake probes, nomenclature and distances involved [mm].

The velocity profiles are presented on Figure 8 for each configuration separately. It is visible that the wake of the horizontal stabilizer and part of the fuselage was well captured showing a more pronounced deficit in the flow momentum when compared to the wake of the wing and pods. These velocity profiles could be used for further comparisons with wind tunnel experimental data.

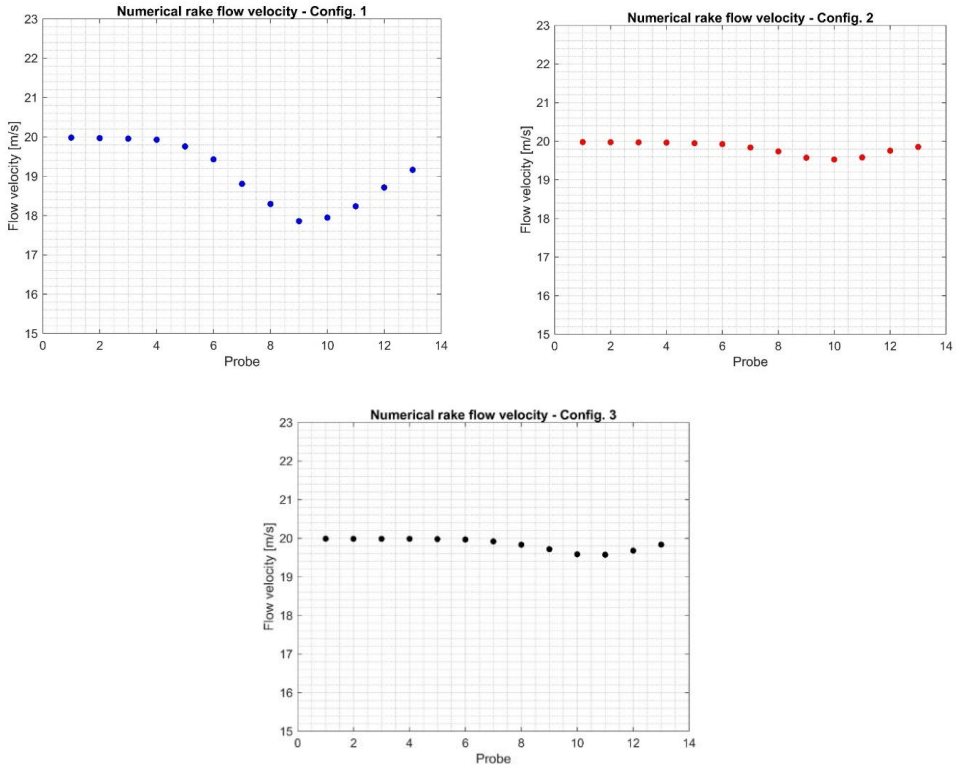

Figure 8. Flow velocity for the rake positions, numerically obtained.

The last aerodynamic parameter analyzed was the drag coefficient that held a value for Mesh 2 of $C_{D,num} = 0.247$. That number is reasonably close to the experimental result from Cicelini (2022), which was $C_{D,exp} = 0.281$. This comparison shows that, although the numerical simulation deviates in some points from the experimental results, it represents the phenomena with notable fidelity. This 12.1% deviation found between the two compared drag coefficients can be explained by many factors, some of them being the well reduced scale of the experimental model, as discussed by Cicelini (2022) and the difficulty in meshing specific regions like the junction between rotors.

4.3 Flow Visualization

To have qualitative data from the flow field, flow visualization was gathered with pathlines over the vehicle by means of the oil flow technique on Fluent Software. As it is shown in Figure 9, it is possible to see a very uniform flow over the fuselage and the mid-sections of the wing (between pods). However, the flow is no longer uniform in the regions of interaction with the pods and in the rear part of the fuselage, close to the engine installation.

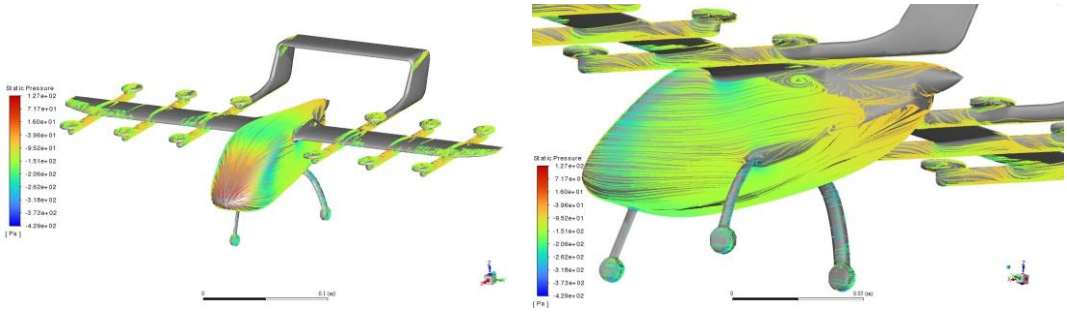

Figure 9. Surface pathlines, “oil flow”, on the E-vtol model.

Figure 10 shows a comparison between the numerical simulation and experimental data from flow visualization gathered by Cicelini (2022), by showing the wall shear stress and flow viz or China clay technique – Barlow et al. (1999).

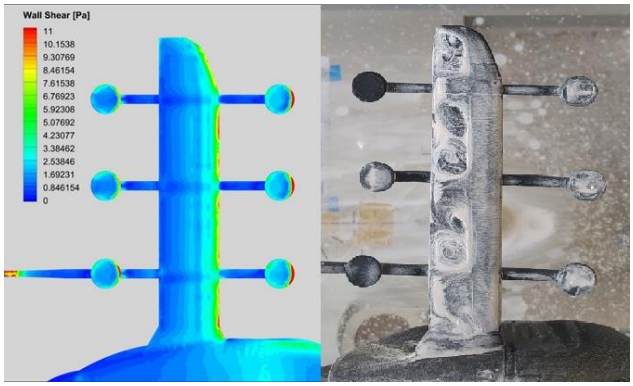

Figure 10. Flow pattern over the wing, CFD (left) and China Clay (right).

5. CONCLUSION

In this study, a comprehensive analysis was undertaken to discern the key attributes that hold the greatest value and feasibility among the prevailing e-VTOL concepts currently under development. This involved a thorough examination of crucial factors pertinent to such a vehicle, including mission profile, passenger safety, efficiency, and practical applicability in real-world scenarios. Building upon this foundation, a novel e-VTOL design was subsequently formulated, leveraging CAD tools, and employing authentic dimensions derived from an initial concept.

A numerical investigation was conducted to analyze the aerodynamics of an e-VTOL concept. The geometry under examination was based on the dimensions of the most promising models currently in development. This conceptual model features fillet surfaces, sharp edges, and streamlined structures. For the numerical analysis, steady simulations using the Reynolds-Averaged Navier-Stokes (RANS) approach were carried out using the commercial software Ansys®, specifically utilizing the Fluent tool and a two-equation Realizable k-ε turbulence model. The solver was equipped with a tetrahedral mesh comprising an average of 6 million elements. All simulations were executed on a system powered by an i7 processor with 12 cores and 48 GB of RAM.

In the numerical process undertaken in this study, the construction of the mesh proved to be the most challenging phase due to the intricacies associated with meshing certain interfaces within the concept, notably the junction between the rotor and its supporting structure. Achieving an acceptable mesh quality necessitated local refinement and numerous iterations. The numerical results were very consistent and showed reasonable value of C_D when compared to experimental data. The analysis of the flow field indicated a uniform and attached boundary layer over the most parts of the model, except in the regions of pods and rear part of fuselage.

This work aims to be a starting point and a reference for general concepts and ideas regarding e-VTOL projects and their aerodynamic study, and it is expected to be a starting point for other deepened studies that will take advantage of CFD modeling to enlighten the flight characteristics of this new modal of transportation.

6. REFERENCES

Stoll, A. M., Bevirt, J., Moore, M. D., Fredericks, W. J., & Borer, N. K., 2014. Drag reduction through distributed electric propulsion. In 14th AIAA aviation technology, integration, and operations conference (p. 2851).

Bacchini, A., & Cestino, E., 2019. Electric VTOL configurations comparison. Aerospace, 6(3), 26.

Simmons, B. M., & Murphy, P. C., 2021. Wind tunnel-based aerodynamic model identification for a tilt-wing, distributed electric propulsion aircraft. In AIAA SciTech 2021 Forum (p. 1298).

Cicelini, G., 2022. Numerical and experimental analysis of the flow over an eVTOL concept.

Almeida, O., 2021. The development of an experimental aerodynamics research center in Brazil. International Journal of Advanced Engineering Research and Science, 8, 3.

ANSYS, Inc., 2016. ANSYS Fluent User's Guide, Release 17.2.

Almeida, O., & Souza, P. R. C., 2017. Flow characterization from a NACA air intake assembled in a canard type aircraft. Revista de Engenharia Térmica, 16(1), 03-10.

Barlow, J. B., Rae, W. H., & Pope, A., 1999. Low-speed wind tunnel testing. John wiley & sons.

7. RESPONSIBILITY NOTICE

The authors are the only responsible for the printed material included in this paper.